Manuscript version: Author's Accepted Manuscript
The version presented in WRAP is the author's accepted manuscript and may differ from the published version or Version of Record.

Persistent WRAP URL:
http://wrap.warwick.ac.uk/114697

How to cite:
Please refer to published version for the most recent bibliographic citation information.
If a published version is known of, the repository item page linked to above, will contain details on accessing it.

Copyright and reuse:
The Warwick Research Archive Portal (WRAP) makes this work by researchers of the University of Warwick available open access under the following conditions.

Copyright © and all moral rights to the version of the paper presented here belong to the individual author(s) and/or other copyright owners. To the extent reasonable and practicable the material made available in WRAP has been checked for eligibility before being made available.

Copies of full items can be used for personal research or study, educational, or not-for-profit purposes without prior permission or charge. Provided that the authors, title and full bibliographic details are credited, a hyperlink and/or URL is given for the original metadata page and the content is not changed in any way.

Publisher's statement:
Please refer to the repository item page, publisher's statement section, for further information.

For more information, please contact the WRAP Team at: wrap@warwick.ac.uk.

A Novel Actuator-Internal Micro/Nano Positioning Stage with an Arch-Shape Bridge Type Amplifier

Fujun Wang, Zhichen Huo, Cunman Liang, Beichao Shi, Yanling Tian, Xingyu Zhao, and
Dawei Zhang

Abstract—**This paper presents a novel actuator-internal two degree-of-freedom (2-DOF) micro/nano positioning stage actuated by piezoelectric (PZT) actuators, which can be used as a fine actuation part in dual-stage system. To compensate the positioning error of coarse stage and achieve a large motion stroke, a symmetrical structure with an arch-shape bridge type amplifier based on single notch circular flexure hinges is proposed and utilized in the positioning stage. Due to the compound bridge arm configuration and compact flexure hinge structure, the amplification mechanism can realize high lateral stiffness and compact structure simultaneously, which is of great importance to protect PZT actuators. The amplification mechanism is integrated into the decoupling mechanism to improve compactness, and to produce decoupled motion in X- and Y- axes. An analytical model is established to explore the static and dynamic characteristics, and the geometric parameters are optimized. The performance of the positioning stage is evaluated through finite element analysis (FEA) and experimental test. The results indicate that the stage can implement 2-DOF decoupled motion with a travel range of 55.4×53.2 μm², and the motion resolution is 8 nm. The stage can be used in probe tip-based micro/nano scratching.**

Index Terms—**Actuator internal configuration, Decoupling mechanism, Micro/nano positioning, Arch-shape bridge type amplifier**

I. INTRODUCTION

MICRO/NANO positioning system has broad applications in biological manipulation, optical fiber alignment, nano-imprint lithography, scanning probe microscopes, micro/nano assembly and etc [1-6]. Compared to conventional macro positioning system, compliant micro/nano positioning system can realize nanometric resolution through the elastic deformation of flexure hinges, which has the advantages of no friction [7-11], no backlash, no lubrication and easy fabrication, whereas the travel range is usually limited from a few microns to several millimeters. In many application fields like probe tip-based micro/nano scratching, there have been quite a few demands of large stroke positioning [12-14], and many efforts have been devoted to realizing high precision and large workspace simultaneously. In order to compensate the positioning error of coarse actuator, the fine actuation part should have the ability to realize nanometric resolution in two perpendicular directions, and the motion stroke should be greater than the minimum resolution of coarse actuator, which is usually about several tens of microns. Furthermore, a compact configuration would be preferable to reduce the system structure size.

In the field of 2-DOF micro/nano positioning, parallel kinematic structure has been widely used because of its high precision, low inertia and compact size [15, 16]. Meanwhile, decoupling mechanisms have been utilized to eliminate or reduce the cross-coupling error. In the literatures, different decoupling mechanisms have been developed to realize both input and output decoupling. Zhu et al designed an XY compliant mechanism with differential actuation mode, which leads to compact structure and high natural frequency, but the motion performance in two directions are inconsistent due to differential actuation principle [17]. Qin et al proposed a decoupled XY stage using statically indeterminate symmetric structure [18]. Xu et al designed a parallel-kinematic XY micro positioning stage based on flexure Roberts mechanism [19]. Generally, the decoupling mechanism would connect serially between motion stage and actuation mechanism, but few studies concentrate on the position configuration relationship among the actuator and its preloaded mechanism, as well as the kinematic decoupling mechanisms in the mechanical design process, which will significantly influence the compactness and

dynamic characteristics of micro/nano positioning system.

Besides the structure configuration, the actuation will also significantly affect the performance of positioning stage. Piezoelectric (PZT) actuator has been commonly used for micro/nano positioning because of its advantages, including large driving force, nanometric resolution and fast response [20]. In some cases, PZT is installed with bolts preloading mechanism to realize high bandwidth, but the limited workspace cannot meet the demand of large stroke positioning. To enlarge the motion stroke, actuation amplification mechanisms have been adopted, like lever mechanism [21], bridge type mechanism [22], Scott-Russell mechanism [23] and differential mechanism [24], where bridge type amplifier has been investigated for wide applications due to its large magnification and compact size. Whereas, the low lateral stiffness of conventional BTA would damage the PZT actuator when bearing undesired external load or motion [25]. To overcome this problem, Li and Xu developed a flexure-based compound bridge type amplifier, which has large lateral stiffness to protect the actuator from undesired external load [26]. Zhu et al investigated a hybrid actuation mechanism with high lateral stiffness and large amplification ratio, which is comprised of Scott-Russell mechanism and half-bridge mechanisms [27]. However, these improved methods would enlarge the size of amplification mechanism, which will affect the compactness and dynamic characteristics of the stage.

In this paper, we developed a novel actuator-internal 2-DOF micro/nano positioning stage, which can be used for micro/nano manufacturing and manipulation, like probe tip-based micro/nano scratching system. The proposed positioning stage adopts the parallel kinematic decoupling mechanism, which can realize input and output decoupling simultaneously. Compared to conventional parallel configuration [10, 18], the actuation mechanism is placed between the decoupling mechanism and motion platform to form an actuation-internal structure, which improves the compactness and dynamic performance. In addition, a novel arch-shape bridge type amplifier (ASBTA) with compact structure and large lateral stiffness is designed to magnify the input displacement and provide actuator-protection function.

The mechanical design of the stage is carried out, and the analytical model of the stage is established to explore the characteristics, which is further verified by finite element analysis (FEA). Experiments have been conducted to evaluate the stage performance. The rest of this paper is organized as follows: the mechanical design of the positioning stage is introduced in Section 2, and the modeling and parameter optimization is performed in Section 3. Section 4 provides the FEA results. In Section 5, experiments are presented to evaluate the performance of the stage. Finally, conclusions are drawn in Section 6.

II. MECHANICAL DESIGN

PZT is adopted as the actuator of the micro/nano positioning stage. In order to achieve large workspace and compact
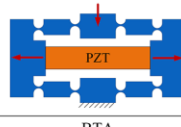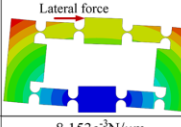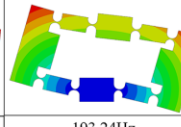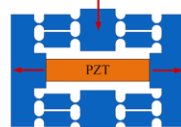

Fig. 1 Comparison of different amplifiers: (a) BTA (b) CBTA, (c) ASBTA.
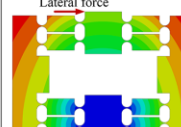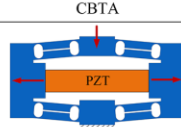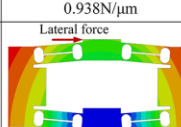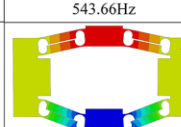
	Actuation mechanism	Lateral stiffness	First vibration mode
(a)	BTA	$8.153e^{-3}N/\mu m$	193.24Hz
(b)	CBTA	$0.938N/\mu m$	543.66Hz
(c)	ASBTA	$0.736N/\mu m$	611.93Hz
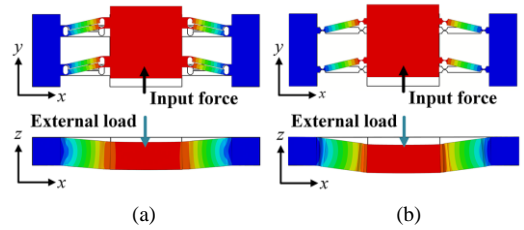
Fig. 2 Compliant prismatic joints: (a) double parallelogram mechanism with SNCFH, and (b) double parallelogram mechanism with right circular flexure hinge.
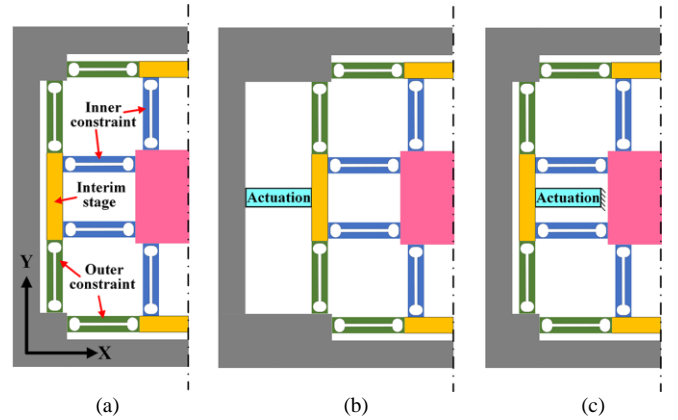
Fig.3 Decoupling mechanism and configuration: (a) decoupling mechanism, (b) actuator-external configuration, and (c) actuator-internal configuration.

structure size, actuation mechanism is required to preload actuator and amplify the output displacement. Many existed stages adopt conventional bridge type amplifier (BTA) as the PZT actuation mechanism as shown in Fig. 1(a) [28]. However, the relatively low lateral stiffness of conventional BTA usually results in undesirable lateral motion when bearing external load, which may damage PZT actuators, and there is an undesired first vibration mode with a low resonant frequency. To overcome the above shortcomings, compound bridge type amplifier mechanism (CBTA) is proposed [26], as shown in Fig. 1(b), which significantly increases the lateral stiffness and the first natural frequency, but the extra bridges with conventional flexure hinges usually result in large dimension size, which enlarges the size of actuation mechanism. Therefore, a novel

Fig. 4 Mechanism of the 2-DOF micro/nano positioning stage

amplification mechanism named ASBTA with compact structure and large lateral stiffness is proposed in this paper to serve as the actuation mechanism, which is composed of two bridge arms with single notch circular flexure hinges (SNCFH), as depicted in Fig. 1(c). The ASBTA actuation mechanism has the structure of two bridges arranged symmetrically to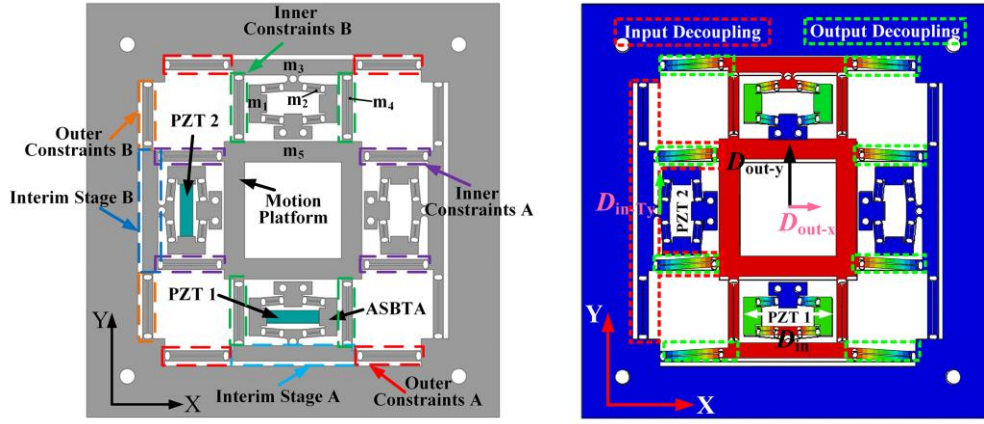 enhance its lateral stiffness, and each bridge consists of a rigid arm and two single notch flexure hinges, which contributes to a compact configuration. Compared to CBTA with the similar feature size in Fig .1(b), the ASBTA not only has the same level lateral stiffness and compact size, but also with a higher first vibration frequency. The symmetrical configuration will contribute to a good guiding performance, and the angle between bridge arms and horizontal line can be adjusted to obtain different amplification ratio and various output displacement direction.

Motion decoupling is an important factor that would significantly influence the performance of multi-DOF positioning. In macro positioning stages, the motion decoupling can be realized through conventional kinematic pairs, which usually has a certain degree of freedom of movement [29, 30], but things are different in micro/nano compliant stages. In order to eliminate the influence of friction and backlash, flexure hinges are adopted, and parallel kinematic configuration is commonly used because of its outstanding performance, but along with the problem of output motion coupling [16]. Ideally, one actuator should only produce one axis output motion to avoid cross-coupling error. In addition, considering that PZT cannot bear large shearing force or moment [25], the actuator should not suffer from undesired loads resulted from the motion of the stage in another axis, which is the input decoupling property. In order to achieve above, a totally decoupled mechanism is designed in this paper.

The totally decoupled mechanism is coming from 2-PP parallel mechanism, where the notations of P represents the prismatic joints. For compliant positioning system, the prismatic joint can be replaced by flexure elements, and should satisfy the demand of high axial stiffness and low shear stiffness. The double parallelogram mechanism possesses excellent guiding ability to serve as prismatic joint, and the characteristic is investigated by FEA. As shown in Fig. 2(a), the double parallelogram mechanism with SNCFH can produce translational motion in Y axis at the end of the mechanism, and the coupling displacement is eliminated due to the symmetrical structure. Compared to double parallelogram mechanism with

right circular flexure hinge in Fig. 2(b), the equivalent decoupling mechanism in Fig. 2(a) has higher stiffness when external force is imposed on motion platform along Z direction, which exhibits better bearing capacity.

The interim stage is established in decoupling mechanism, and the double parallelogram mechanism with SNCFH is arranged orthogonally as inner and outer constraints. As depicted in Fig.3 (a), the outer constraint will connect the interim stage and base, and the inner constraint will connect the interim stage and motion platform. As actuation part is connected with interim stage, the input end would keep stable in Y direction due to the high axial stiffness of outer constraint, which can protect the actuator from shear force. Moreover, the constraints will also serve as guiding mechanism to achieve output decoupling. Generally, most of the micro/nano positioning stages adopt the configuration that actuation part is placed at the outside of interim stage. As can be seen in Fig. 3(b), the actuation is between interim stage and base, and the output displacement would be transferred through interim stage and inner constraint. However, the outer actuation mechanism could enlarge the stage structure size, which cannot satisfy the compactness in some occasions. The stage in this paper utilizes an actuator-internal configuration, as shown in Fig. 3(c). The actuation part is placed between interim stage and motion platform, which not only has good decoupling property, but also with a compact size and better dynamic performance.

From the above, the schematic diagram of the stage is depicted in Fig. 4. The structure consists of ASBTA, PZT actuators, outer constraints, inner constraints, interim stages and motion platform. A symmetric configuration is adopted to avoid coupling error. When the PZT 1 is actuated, the input displacement D_{in} will be amplified and transferred to interim stage A through ASBTA. By reason of the high longitudinal stiffness of single notch circular flexure hinges, the amplified displacement will be delivered to motion platform through inner constraint B, and the inner constraint A will serve as the guiding mechanism to ensure the motion platform moving in Y axis, which can achieve output decoupling. Meanwhile, the interim stage B will remain stable due to the high axial stiffness of outer constrain B, which can avoid undesired lateral loads on input end. Because of the symmetry, the driven process along X axis is similar. Therefore, the input and output decoupling will be realized simultaneously.

III. ANALYTICAL MODELING AND PARAMETER OPTIMIZATION

A. Static modeling

To analyze the input stiffness and amplification, the modeling is based on Euler-Bernoulli beam theory and compliance matrix method. The compliance of prismatic beam is considered, and the flexure hinges are considered to have 3-DOF. The compliance matrix of SNCFH and prismatic beam can be written as

$$C = \begin{bmatrix} C_{11} & 0 & 0 \\ 0 & C_{22} & C_{23} \\ 0 & C_{32} & C_{33} \end{bmatrix} \quad (1)$$

where C_{ij} $(i,j=1,2,3)$ are the parameters of compliance matrix.

The compliance matrix of SNCFH and prismatic beam will be denoted as C_S and C_P respectively, and the matrix parameters can be derived by Castigliano's displacement theorem [31]. The geometric parameters of SNCFH and prismatic beam are shown in Fig. 5.

According to the compliant mechanism theory, the compliance equation of the flexure hinge can be obtained as

$$D = \begin{bmatrix} x_1 \\ y_1 \\ \theta_{z1} \end{bmatrix} = \begin{bmatrix} C_{11} & 0 & 0 \\ 0 & C_{22} & C_{23} \\ 0 & C_{32} & C_{33} \end{bmatrix} \begin{bmatrix} F_{x1} \\ F_{y1} \\ M_{z1} \end{bmatrix} = CF \quad (2)$$

where D is the displacement vector $[x_1, y_1, \theta_{z1}]$, F is the external force vector $[F_{x1}, F_{y1}, M_{z1}]$. To obtain the stage compliance, the compliance matrix of flexure hinge will be transferred from local coordinate O_i-xy to target coordinate O_j-xy by

$$C_{Oj} = T_i^j C_{Oi} \left(T_i^j\right)^T \quad (3)$$

$$T_i^j = R_i^j P_i^j = \begin{bmatrix} r_{11} & r_{12} & r_{13} \\ r_{21} & r_{22} & r_{23} \\ r_{31} & r_{32} & r_{33} \end{bmatrix} \begin{bmatrix} 1 & 0 & p_y \\ 0 & 1 & -p_x \\ 0 & 0 & 1 \end{bmatrix} \quad (4)$$

where R_i^j and P_i^j represent the rotation matrix and translation matrix from coordinate O_i-xy to O_j-xy respectively, and $[p_x, p_y]^T$ is the position vector $\overrightarrow{O_iO_j}$ in coordinate O_i-xy.

As the actuation mechanism, ASBTA would significantly influence the performance of positioning stage, which will be analyzed at first. Assuming that the actuation mechanism is connected to rigid ground at one end, which can be seen in Fig. 6. Due to the symmetrical structure, the amplifier can be divided as left part and right part, and ASBTA is parallelly connected by two parts at point F.

In the right half part, two chains are connected serially, and each chain is comprised of two linkages. The compliance of right-down part at point F can be derived by

$$_{right\_link1}C_F = T_{O_1}^F C_S (T_{O_1}^F)^T + T_{O_2}^F C_S (T_{O_2}^F)^T + T_{O_5}^F C_P (T_{O_5}^F)^T \quad (5)$$

$$_{right\_link2}C_F = T_{O_3}^F C_S (T_{O_3}^F)^T + T_{O_4}^F C_S (T_{O_4}^F)^T + T_{O_6}^F C_P (T_{O_6}^F)^T \quad (6)$$

$$_{right-down}C_F = (_{right\_link1}C_F^{-1} + _{right\_link2}C_F^{-1})^{-1} \quad (7)$$

In the same way, the compliance of right-top part at point F can be obtained.

$$_{right-top}C_F = (_{right\_link3}C_F^{-1} + _{right\_link4}C_F^{-1})^{-1} \quad (8)$$

In view of the serial connection between two chains, the compliance of the right part at output end F can be written as
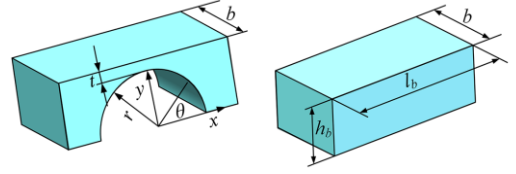

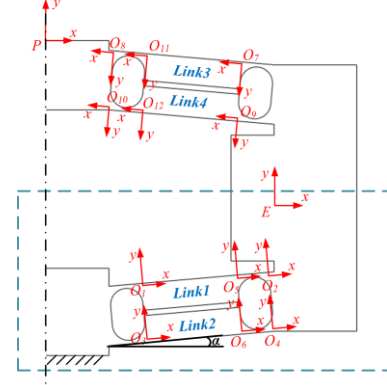Fig. 5 Single notch circular flexure hinge and prismatic beam

Fig. 6 Parameters and coordinates for half of ASBTA.

$$_{right}C_F = _{right-down}C_F + _{right-down}C_F \quad (9)$$

Due to the left-right symmetry of actuation mechanism, the compliance of ASBTA at point F can be obtained as

$$C_F = \left[\left(_{right}C_F\right)^{-1} + \left(R_y(\pi) _{right}C_F R_y(\pi)^T\right)^{-1} \right]^{-1} \quad (10)$$

where $R_y(\pi)$ is the transformation matrix from the right to the left section. It can be obtained that $C_F(2,2)$ is the output compliance of ASBTA, which reveals the relationship between transformation and external force at the output end.

When considering the input compliance of ASBTA, only one quarter of actuation mechanism is analyzed due to the symmetrical structure, as can be seen in Fig 6. Similar to the output compliance, the compliance of one quarter structure at point E can be calculated as

$$_{link1}C_E = T_{O_1}^E C_S (T_{O_1}^E)^T + T_{O_2}^E C_S (T_{O_2}^E)^T + T_{O_5}^E C_P (T_{O_5}^E)^T \quad (11)$$

$$_{link2}C_E = T_{O_3}^E C_S (T_{O_3}^E)^T + T_{O_4}^E C_S (T_{O_4}^E)^T + T_{O_6}^E C_P (T_{O_6}^E)^T \quad (12)$$

$$_{right\_down}C_E = (_{link1}C_E^{-1} + _{link2}C_E^{-1})^{-1} \quad (13)$$

According to the force equilibrium theory and compliance matrix method, the following relationships can be obtained:

$$\Delta x = \frac{1}{2}C_E(1,1)F_{in} + \frac{1}{2}C_E(1,2)F_{out} + C_E(1,3)M_z \quad (14)$$

$$\Delta y = \frac{1}{2}C_E(2,1)F_{in} + \frac{1}{2}C_E(2,2)F_{out} + C_E(2,3)M_z \quad (15)$$

$$\Delta\theta = \frac{1}{2}C_E(3,1)F_{in} + \frac{1}{2}C_E(3,2)F_{out} + C_E(3,3)M_z \quad (16)$$

where F_{in} is the input force, F_{out} is the equivalent external force at the output end of ASBTA, and M_z is the equivalent moment. Based on the working principle, the rotation of end point E is zero, and the following relationship can be obtained:

$$\Delta\theta_z = 0 \quad (17)$$

As the decoupling mechanism is serially connected with actuation mechanism, the influence of decoupling mechanism can be simplified as an external load which imposed at the output end of ASBTA. The compliance of decoupling mechanism will be deduced by Euler-Bernoulli beam theory.

The SNCFH in decoupling mechanism can be simplified as a revolute pivot with a torsional spring. For one arm of decoupling mechanism, the external force is F_y. Due to the symmetricity, only half of the structure will be analyzed. The reaction force and moments are denoted by F_{AY}, M_A, and M_O respectively, as shown in Fig. 7.

From static equilibrium conditions, the following equations can be obtained:

$$F_{Ay} + F_y = 0 \tag{18}$$

$$M_A - F_y(2l_1 + l_2 + l_3) - M_O = 0 \tag{19}$$

The angular and linear deflections at point B, D and O can be calculated as

$$\begin{bmatrix} \Delta y_B \\ \theta_B \end{bmatrix} = \begin{bmatrix} C_{22} & C_{23} \\ C_{32} & C_{33} \end{bmatrix} \begin{bmatrix} F_y \\ F_y(l_1 + l_2 + l_3) + M_O \end{bmatrix} \tag{20}$$

$$\begin{bmatrix} \Delta y_D \\ \theta_D \end{bmatrix} = \begin{bmatrix} C_{22} & C_{23} \\ C_{32} & C_{33} \end{bmatrix} \begin{bmatrix} F_y \\ F_y l_3 + M_O \end{bmatrix} + \begin{bmatrix} 1 & l_1 + l_2 \\ 0 & 1 \end{bmatrix} \begin{bmatrix} \Delta y_B \\ \theta_B \end{bmatrix} \tag{21}$$

Considering the boundary conditions $\theta_o=0$, and $\theta_o=\theta_D$, the moment M_O and the linear compliance of decoupling arm c_r in Y direction can be derived as

$$M_o = -\frac{F_y[2C_{32} + C_{33}(l_1 + l_2 + 2l_3)]}{2C_{33}} \tag{22}$$

$$c_r = 2C_{22} + 2C_{23}(l_1 + l_2 + l_3) + C_{33}(l_1 + l_2 + l_3)(l_1 + l_2)$$
$$- \frac{[2C_{32} + C_{33}(l_1 + l_2 + 2l_3)][2C_{23} + C_{33}(l_1 + l_2)]}{2C_{33}} \tag{23}$$

Because the dimensions of decoupling arms are different in outer and inner constraints, the linear compliance is also different. We define the compliance of two kinds of constraints is c_{r1} and c_{r2} respectively, which can be obtained from (20). As the decoupling part is composed of decoupling mechanism and another bridge type mechanism parallel connecting together, the compliance of decoupling part c_e can be obtained.

$$c_e = ((8c_{r1})^{-1} + (8c_{r2})^{-1} + (C_F(2,2))^{-1})^{-1} \tag{24}$$

As the reaction force exerted on decoupling part is F_{out}, Then the relationship between output motion and equivalent external force can be written as

$$2\Delta y = F_{out}c_e \tag{25}$$

In view of the boundary conditions with (17) and (25), recall (14,15,16), the amplification ratio and input stiffness of the stage can be calculated as

$$A_r = \frac{\Delta y}{\Delta x} = \frac{C_E(2,1) + C_E(2,2)d_1 + 2C_E(2,3)d_2}{C_E(3,1) + C_E(3,2)d_1 + 2C_E(3,3)d_2} \tag{26}$$

$$k_{in} = \frac{F_x}{2\Delta x} = \frac{1}{C_E(1,1) + C_E(1,2)d_1 + 2C_E(1,3)d_2} \tag{27}$$

where

$$d_1 = \frac{C_E(2,1)}{c_e - C_E(2,2)} -$$
$$\frac{2C_E(2,3)C_E(3,1)(c_e - C_E(2,2)) + C_E(3,2)C_E(2,1)}{(c_e - C_E(2,2))^2(2C_E(3,3) + 2C_E(3,2)C_E(2,3))} \tag{28}$$

$$d_2 = -\frac{C_E(3,1)(c_e - C_E(2,2)) + C_E(3,2)C_E(2,1)}{2C_E(3,3)(c_e - C_E(2,2)) + 2C_E(3,2)C_E(2,3)} \tag{29}$$
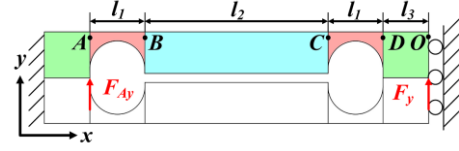

Fig. 7 The equivalent structure of decoupling mechanism.

It has been noted that the maximum stress usually occurs at the outermost surface of the thinnest portion of the flexure hinge which has the maximum rotation angle. The maximum stress of SNCFH [32] can be calculated as

$$\sigma_{max} = \left| \frac{2\sqrt{2}Et^{1/2}}{3\pi r}\varphi_{max} \right| + \left| \frac{F_{max}}{bt} \right| \tag{30}$$

where r, t and b denote the radius, thickness and height of SNCFH respectively, E is the elastic modulus of the material, φ_{max} and F_{max} are the maximum rotation angle and axial force.

According to the kinematic relationship of the stage, the flexure hinge with the maximum rotation angle is the SNCFH in bridge type amplification. The maximum rotation angle and axial force can be derived as

$$\varphi_{max} = \frac{u_{in}A_r}{2l_b} \tag{31}$$

$$F_{max} = \frac{u_{in}k_{in}\cos(\alpha)}{4} \tag{32}$$

where u_{in} is the input displacement from PZT.

B. Dynamic modeling

As the mass of flexure hinge is relatively small, the kinetic energy of flexure hinge is neglected. Due to the symmetric configuration and good decoupling properties of the stage, dynamic analysis is only carried out in x axis. The generalized coordinate is selected as the input displacement u_{in}.

The kinetic energy of the stage can be divided into two parts, the kinetic energy of bridge type amplifier and outer mechanism, which are denoted as T_B and T_O respectively.

$$T_B = (\frac{m_1}{4} + \frac{m_2}{4})(\dot{u}_{in})^2 + 4J_1(\frac{A_r\dot{u}_{in}}{2l_e})^2 + (\frac{5}{4}m_2 + \frac{1}{2}m_3)(A_r\dot{u}_{in})^2 \tag{33}$$

$$T_O = (2m_4 + 4m_4 + \frac{m_5}{2})(A_r\dot{u}_{in})^2 + 8J_2(\frac{A_r\dot{u}_{in}}{l_f})^2 \tag{34}$$

$$T = T_B + T_O \tag{35}$$

where m_i is the mass of the linkages in the stage; J_1 and J_2 represent the rotational inertia of linkages in bridge type amplifier and guiding mechanism respectively.

Based on virtual work principle, the potential energy is

$$V = \frac{1}{2}k_{in}u_{in}^2 \tag{36}$$

Substituting the kinetic and potential energies into Lagrange equation [27]

$$\frac{d}{dt}(\frac{\partial T}{\partial \dot{u}_{in}}) - \frac{\partial T}{\partial \dot{u}_{in}} + \frac{\partial V}{\partial \dot{u}_{in}} = F \tag{37}$$

The dynamic equation can be described as

$$M\ddot{u}_{in} + k_{in}u_{in} = 0 \tag{38}$$

where the equivalent mass M can be derived by

$$M = \frac{\partial T}{\partial \dot{u}_{in}}\frac{1}{\dot{u}_{in}} \tag{39}$$

TABLE I
DIMENSIONS AND CHARACTERISTICS OF OPTIMIZED POSITIONING STAGE

Parameter (mm)	ASBTA					
	r_1	t_1	b	l_b	h_b	α
Value	0.9	0.2	12	5.34	1.5	5°
Parameter (mm)	Decoupling mechanism					
	r_2	t_2	l_1	l_2	l_{3outer}	l_{3inner}
Value	1	0.3	2	21	1	2
Parameter	f		A_r		k_{in}	σ_{max}
Value	315.9Hz		6.49		28.3N/μm	94.34Mpa

TABLE II
PHYSICAL PARAMETERS OF MATERIAL

Material parameter	E (GPa)	v	ρ (kg/m^3)
value	71.1	0.33	2810

Based on the theory of vibration, the translational natural frequency can be calculated as

$$f = \frac{1}{2\pi}\sqrt{\frac{k_{in}}{M}} \qquad (40)$$

C. Parameter optimization

In the field of tip-based micro/nano scratching, the working frequency is usually below 10 Hz to protect the probe, and the dynamic performance of positioning stage is important in scratching. Therefore, the first natural frequency is selected as the objective function to suppress the potential vibration and improve machining stability. As the main purpose of proposed positioning stage is to compensate the coarse positioning error and implement high precision motion, the motion stroke should be no less than 50 μm while the extension range of selected PZT actuator is about 10 μm under preloading condition. Because the input stiffness would affect the output of PZT actuator, the boundary condition is settled as $k_{in}<0.5k_{PZT}$ [27]. In addition, the maximum stress of the flexure hinge should be less than the allowable stress of the material.

The optimization work can be concluded as follows:
1) Objective: Maximize the first natural frequency (*f*).
2) Related parameters: r_i, t_i, and α.
3) Subject to:
   a) amplification ratio: $A_r \geqslant 5$;
   b) input stiffness: $k_{in}<0.5k_{PZT}$ ($k_{PZT} = 60$ N/μm)
   c) constraint equations: $\sigma_{max} < \sigma_m/s_f$ (σ_m=400 MPa, s_f =2.5)
   d) parameters range: 0.8 mm < r_i <1.5 mm, 0.15 mm< t_i <0.5 mm, 3°< α <8°.

The dimension parameter of PZT actuator is 5×5×18 mm^3, and the rest parameters of the stage are determined based on the geometric relationship. The optimization process is conducted in MATLAB via genetic algorithm (GA) optimization toolbox with the initial value [r_1, t_1, r_2, t_2, α] = [1, 0.3, 1.2, 0.3, 6°]. The dimensions and characteristics of optimized positioning stage are listed in Table I.

IV. FINITE ELEMENT ANALYSIS

Finite element method (FEM) is used to analyze the static and dynamic characteristics of the stage. The material of the stage is AL7075, and the corresponding physical parameters are listed in Table II.

The Y-axis deformation behavior of the stage is presented in Fig.8 with an input displacement of 10 μm. The FEA result indicates that the output displacement is 59.4 μm and the
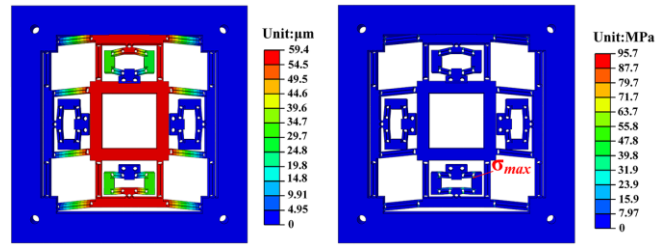

Fig. 8 The deformation result by FEA.
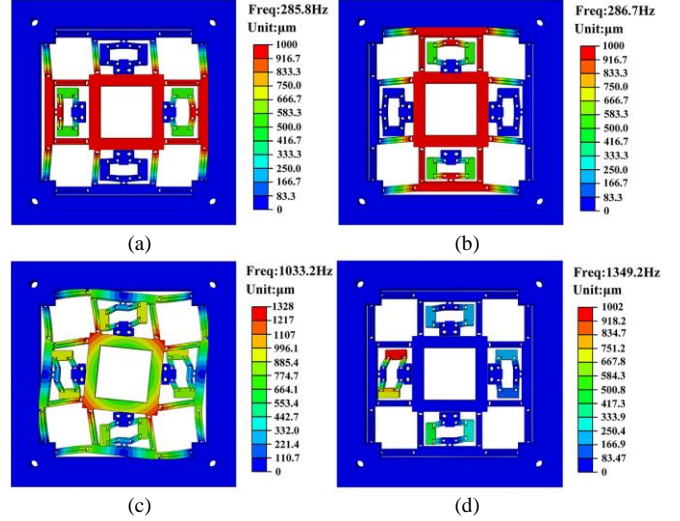

(a)　　　　　　　(b)

(c)　　　　　　　(d)

Fig. 9 The first four modal shapes of the stage. (a) Mode 1, (b) Mode 2, (c) Mode 3, and (d) Mode 4.

displacements in two directions are decoupled well. The maximum stress is 95.7 MPa. It can be observed that the maximum stress is far below the yield stress (503 MPa) of the material. To get the input stiffness of the stage, a constant force of *F*=100 N is exerted at the input end of actuation mechanism. The input stiffness can be calculated as k_{in}=24.9 N/μm.

The vibration frequency and mode of the stage is analyzed. Fig. 9 demonstrates that the first four natural frequencies of the proposed stage are 285.8 Hz, 286.7 Hz, 1033.2 Hz and 1349.2 Hz respectively. The first two mode shape is the translation motion along the center line of the X axis and Y axis, the third mode shape is displayed with motion stage rotates around Z axis, and the forth mode shape shows the swing up and down at the input sides of actuation mechanism. As the natural frequency of undesired modes is much larger than working modes, the stage exhibits good dynamic performance.

V. EXPERIMENTS AND DISCUSSIONS

A. Experimental setup

A prototype of the stage is fabricated monolithically through wire electrical discharge machining (wire EDM). The overall dimension of the stage is 160×160×12 mm^3, and the dimension of the working platform is 54×54 mm^2. Two PZTs (PSt150/5×5×20L from COREMORROW, Inc.) are inserted into the bridge type amplifier to drive the stage. A dSPACE DS1103 controller is utilized to produce analog voltages, which are then amplified by THORLABS voltages amplifier to provide voltages of 0-100 V for the drives of PZTs. The displacements of the stage are measured by three capacitive sensors (C8-2.0 Lion, Inc.), whose outputs are collected
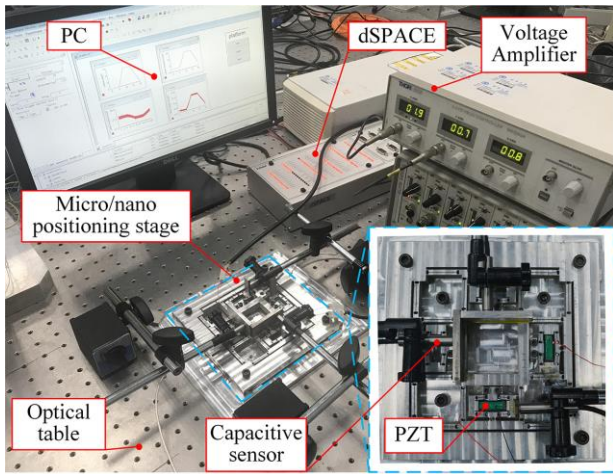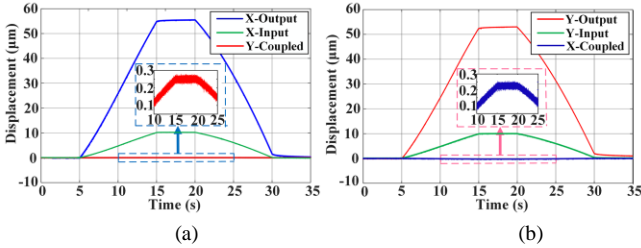
Fig. 10 Experimental setup.

(a)   (b)

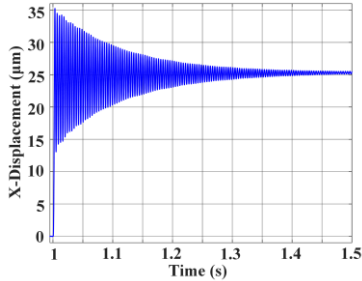Fig. 11 Open loop travel range: (a) X-direction, and (b) Y-direction.

Fig. 12 Open-loop step response

(a)   (b)

Fig. 13 Frequency response of the stage: (a) X-axis, and (b) Y-axis.

(a)   (b)

Fig. 14 Cross-coupling response of the stage: (a) cross-coupling relative to X-axis, and (b) cross-coupling relative to Y-axis.

(a)   (b)

Fig. 15 Hysteresis curve (a) Output displacement, and (b) Cross-coupling error.

simultaneously by a computer through dSPACE controller. All the devices are mounted on a Newport RS-4000 optical table to reduce the external disturbance effects, and the experimental setup is shown in Fig. 10.

B. Open-loop experimental test

First of all, the open-loop properties are experimentally tested. The PZT actuators are actuated with a trapezoid voltage signal with slope of 10 V/s and maximum voltage of 100 V under open-loop condition. Sensor targets are attached at the input and output end of the stage, where two output sensor targets are configured orthogonally to measure the output and coupling displacement. Three capacitive sensors are utilized to measure the displacement of sensor targets, and the results are illustrated in Fig. 11. It can be observed that the workspace of the stage is 55.4×53.2 μm². The X-axis amplification ratio is 5.46, while the coupling rate in Y axis is 0.45%; the amplification ratio in Y axis is 5.37, while the coupling rate in X axis is 0.42 %. The measured coupling ratio is relatively small, which indicates good decoupling properties.

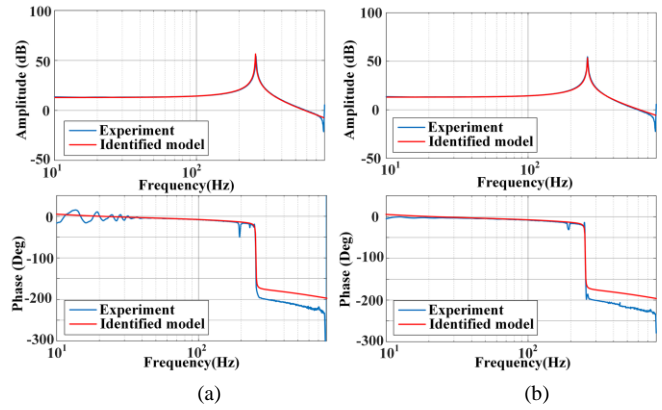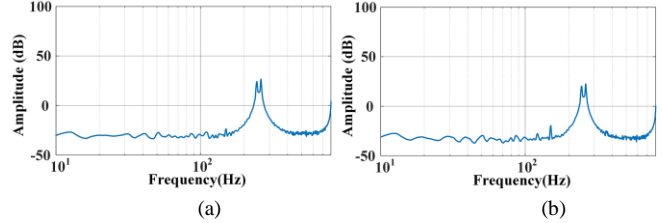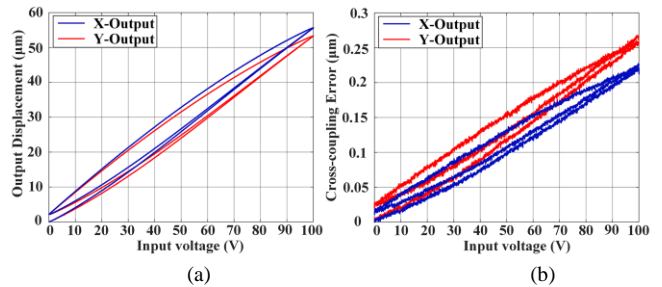The step responses of the stage are investigated, and the experimental result of X axis is depicted in Fig. 12. When the step voltage with amplitude of 50 V is applied on actuator, it can be obtained that the setting time is 0.35 s.

To evaluate the dynamic performance of the stage, the sine swept signal with a constant voltage of 0.5 V and a frequency varying from 0.1 Hz to 800 Hz is applied to PZT actuators in two directions respectively. The bode diagram of the transfer function is plotted in Fig. 13. It can be found that the first two resonance frequency is 253.4 Hz and 253.6 Hz respectively, which matches well with the FEA. The cross-coupling response is plotted in Fig. 14, and the coupling motion is 42 dB and 45 dB smaller than the primary motion in X- and Y- axes respectively.

Due to the PZT actuators, the hysteresis and nonlinearity of the stage is obvious under open-loop system [33, 34]. The hysteresis curve and corresponding cross-coupling error are depicted in Fig. 15 according to the relationship between input voltage and output displacement. It can be seen that for a given input voltage value, there are two corresponding displacements in the extension and retraction process of PZT actuators.

C. Closed-loop experimental test

To improve the linearity and repeatability of motion transmission, Proportional-Integral-Derivative (PID) controller
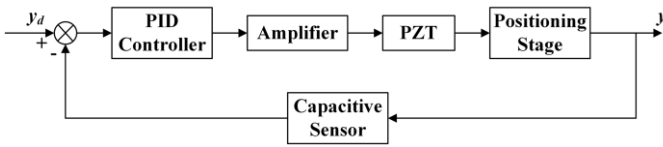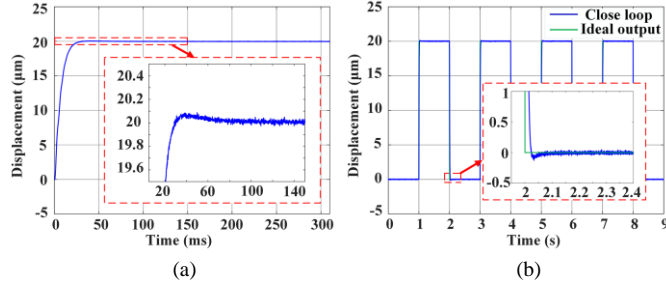
Fig. 16 Block diagram of feedback controller.

(a)

(b)

Fig. 17 Output displacement under close-loop control in X direction. (a) Step response, and (b) Square motion tracking.
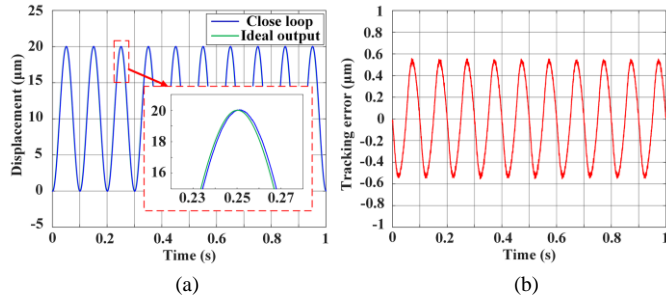

(a)

(b)

Fig. 18 Trajectory tracking with 10 Hz sinusoidal signal. (a) Tracking results, and (b) Tracking error.

is utilized to compensate the hysteresis that exists in PZT actuators. The block diagram of feedback controller is shown in Fig. 16, where the output displacement is measured by capacitive sensors, and the positioning error between actual output value and desired value is defined as $e_d=y_d-y$. The controlling model is established by using the MATLAB/Simulink and downloaded to the dSPACE control system. The PID controller can be expressed as

$$u_d(t) = K_P e_d(t) + K_I \int_0^t e_d(t)dt + K_D \frac{de_d(t)}{dt} \qquad (41)$$

where K_P, K_I and K_D denote the proportional gain, integral gain and differential gain respectively.

Based on Ziegler-Nichols method, the parameters of PID controller are tuned as: k_p=0.1, k_i=40, k_d=0.000064. The step response under PID control is depicted in Fig. 17(a), and the amplitude of the step is 20 μm. The settling time is 80 ms, and overshoot is 0.1 μm. The square motion-tracking performance is also tested, and the amplitude is 20 μm. The result shown in Fig. 17(b) indicates that the stage can provide high precision positioning under closed-loop control.

The signal trajectory tracking ability is tested. For the applications of probe tip-based micro/nano scratching, the working frequency is usually below 10 Hz. So during the test, with a single 10 Hz sinusoidal input signal applied to X-axis actuator, the ideal output displacement and actual trajectory are depicted in Fig. 18(a), and the tracking error is shown in Fig. 18(b). It can be obtained that the maximum tracking error along x axis is ±0.57 μm, which is 5.7% of the motion stroke. To verify the motion linearity, a 10 Hz triangular input signal with an amplitude of 20 μm is applied, and the results are plotted in
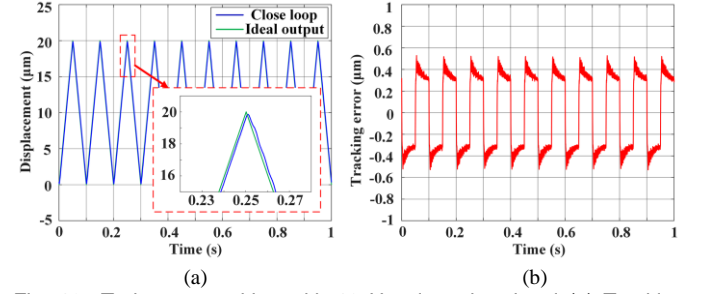
Fig 19. As the measured output displacement can closely

(a)

(b)

Fig. 19 Trajectory tracking with 10 Hz triangular signal (a) Tracking results, and (b) Tracking error.
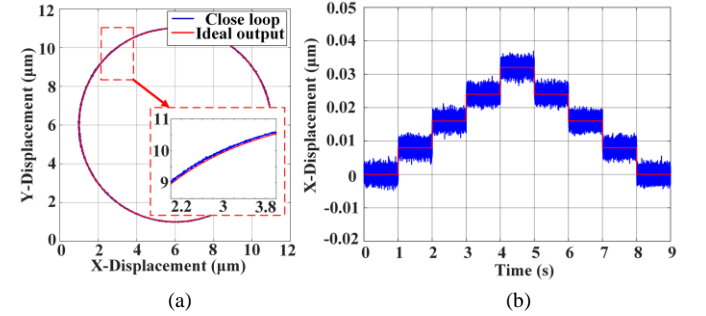

(a)

(b)

Fig. 20 (a) Circle trajectory experiment, and (b) Multi-step response for resolution experiment

TABLE III
COMPARISONS WITH DEVELOPED POSITIONING STAGES

Ref	Dimension (mm²)	Bandwidth (Hz)	Workspace (μm²)	Amplification Ratio	Actuator Protection
[18]	230×230	665.4	8×8	1	NO
[16]	155×155	2k	19×19	1	NO
[21]	185×185	423	82×82	2.1	NO
[26]	300×300	233.83	101×101	5.07	YES
[22]	250×250	110.2	117×117	5.85	YES
This work	160×160	253.4	55.4×53.2	5.37	YES

follow the ideal triangular trajectory, the hysteresis of PZT actuator is effectively eliminated.

To test the tracking capability of two axis simultaneously, a typical circle trajectory experiment is conducted. The trajectory can be expressed as

$$x = 5\sin(20\pi t - 0.5\pi) + 6$$
$$y = 5\sin(20\pi t) + 6 \qquad (42)$$

As can be seen in Fig. 20(a), the stage can accurately track the desired trajectory under close-loop control, which indicates that the PID controller can eliminate the hysteresis and nonlinearity, and further improve the positioning accuracy.

The resolution of the stage is tested, and the result is shown in Fig. 20(b), the resolution is 8 nm from the multi-step response experiment, which indicates the stage can realize nanometric resolution over tens of microns working range.

D. Performance evaluation and discussion

Comparison study has been carried out with some typical fine stages that can be used for coarse/fine positioning system and the results are shown in Table III. In the field of micro/nano positioning, factors like workspace, resonant frequencies and physical size are commonly used to assess a positioning stage. In addition, another factor should be considered is the actuator protection device, which is of great importance to protect PZT from undesired motion or load. It can be obtained that the

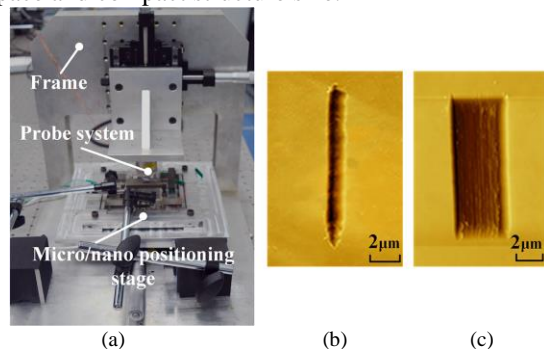proposed stage can not only protect actuator, but also with large workspace and compact structure size.

Fig. 21 Scratching experiment. (a) Micro/nano scratching system, (b) Single groove scratching, and (c) Multi-groove scratching

E. Probe tip-based micro/nano scratching

To investigate the performance of proposed stage in application, the experiment is conducted by using positioning stage in a self-developed micro/nano scratching system shown in Fig. 21(a). The overall frame applies the gantry structure, and three manual coarse motion platforms are arranged orthogonally to realize a large range adjustment. The micro/nano positioning stage is placed on the planer coarse motion platform to realize precision positioning, and the sample is placed on micro/nano positioning stage. An L-shape bracket is fixed on vertical manual coarse positioning platform, and the horizontal plate is utilized to connect the probe system. After the probe is indented into the sample, the micro/nano positioning stage would be actuated to complete the scratching process. The result of single groove scratching on a silicon substrate is depicted in Fig. 21(b). In order to investigate the precision positioning ability in scratching, the multi-groove scratching with 40 nm feed is conducted, which can be seen in Fig. 21(c). The experiments indicate that proposed stage can not only compensate the positioning error of coarse motion platform, but also implement stable and precision motion in tip-based micro/nano scratching process.

VI. CONCLUSION

In this paper, we present the design, modeling, analysis and experimental test of a novel actuator internal 2-DOF micro/nano positioning stage. The input displacement is amplified by an arch-shape bridge type amplifier based on single notch circular flexure hinges, which is designed with compact structure and large transverse stiffness. Double parallel mechanism is adopted to realize input and output decoupling. In addition, an actuation internal configuration is utilized to reduce the structure size. The analytical model is established to analyze the characteristics of the stage and optimize the geometric parameters. Furthermore, FEA is utilized to evaluate the performance of the positioning stage.

A prototype of this stage is fabricated by EDM method, and a series of experiments are conducted. The experimental results indicate that the proposed positioning stage can implement decoupled motion with the travel range of 55.4×53.2 μm^2, where the amplification ratio in X and Y axis is 5.46 and 5.37 respectively. PID controller is utilized to improve the motion

stability and repeatability. The comparison with some typical stages indicates that proposed positioning stage can not only provide actuator-protection function, but also realize large workspace and compact configuration simultaneously. Micro/nano scratching experiments have been conducted based on the self-developed micro/nano scratching system, which indicates that proposed stage can be utilized in the field of probe tip-based micro/nano scratching. The main focus of future study is to investigate more complex scratching and manipulation with the proposed stage.

REFERENCES

[1] X. Chen and Y. Li, "Design and analysis of a new high precision decoupled XY compact parallel micromanipulator," *Micromachines*, vol. 8, no. 82, pp. 1–13, Mar. 2017.

[2] C. Liang, F. Wang, Q. Yang, Y. Tian, X. Zhao and D. Zhang, "Design and characteristic analysis of an aerostatic decoupling table for microelectronic packaging", *PIMechE, Part C, Journal of Mechanical Engineering Science*, vol. 232, no.6, pp. 1079-1090, 2018.

[3] F. Wang, Z. Ma, W. Gao, X. Zhao, Y. Tian, D. Zhang and C. Liang, "Dynamic modeling and control of a novel XY positioning stage for semiconductor packaging", *Transactions of the Institute of Measurement and Control*, vol. 37, no.2, pp. 177-189, 2015.

[4] T, Tuma, W, Haeberle, H. Rothuizen, J. Lygeros, A. Pantazi, and A. Sebastian, "Dual-stage nanopositioning for high-speed scanning probe microscopy," *IEEE/ASME Trans. Mechatronics*, vol. 19, no. 13, pp. 1034-1045, Jun. 2014.

[5] S. Polit and J. Dong, "Development of a high-bandwidth XY nanopositioning stage for high-rate micro-nanomanufacturing," *IEEE/ASME Trans. Mechatronics*, vol. 16, no. 4, pp. 724–733, Aug. 2011.

[6] G. Schitter, K. J. Astrom, B. DeMartini, P. J. Thurner, K. L. Turner, and P. K. Hansma, "Design and modeling of a high-speed AFM-scanner," *IEEE Trans. Control Syst. Technol.*, vol. 15, no. 5, pp. 906–915, Sep. 2007.

[7] F. Wang, J. Li, S. Liu, and X. Zhao, D. Zhang and Y. Tian, "An improved adaptive genetic algorithm for image segmentation and vision alignment used in microelectronic bonding", *IEEE/ASME Trans. Mechatronics*, vol. 19, no. 3, pp. 916-923, 2014.

[8] C. Liang, F. Wang, Y. Tian, X. Zhao and D. Zhang, "Development of a high speed and precision wire clamp with both position and force regulations", *Robot Comput-Integr Manuf*, vol. 44, pp. 208-217, 2017.

[9] F. Wang, C. Liang, Y. Tian, X. Zhao and D. Zhang, "Design and control of a compliant microgripper with a large amplification ratio for high-speed micro manipulation", *IEEE/ASME Trans. Mechatronics*, vol. 21, no. 3, pp. 1262-1271, 2016.

[10] Y. K. Yong, B. Bhikkaji, S. O. R. Moheimani, Design, modeling, and FPAA-based control of a high-speed atomic force microscope nanopositioner, *IEEE/ASME Trans. Mechatronics*, vol. 18, no. 3, pp. 1060-1071, Jun. 2013.

[11] Z. Guo, Y. Tian, X. Liu, F. Wang, C. Zhou, and D. Zhang, "Experimental investigation of the tip based micro/nano machining", *Applied Surface Science*, vol. 426, pp406-417, Jul. 2017.

[12] Z. Guo, Y. Tian, X. Liu, F. Wang, C. Zhou, and D. Zhang, "Modeling and simulation of the probe tip based nanochannel scratching," *Precision Engineering*, vol. 49, pp136-145, Feb. 2017

[13] F. Wang, C. Liang, Y. Tian, X. Zhao and D. Zhang, "Design of a piezoelectric- actuated microgripper with a three-stage flexure-based amplification", *IEEE/ASME Trans. Mechatronics,* vol. 20, no. 5, pp. 2205-2213, 2015.

[14] M. Muraoka and S. Sanada. "Displacement amplifier for piezoelectric actuator based on honeycomb link mechanism," *Sensor Actuat A-Phys*, vol. 157, no.1, pp. 84-90, Jan. 2010.

[15] Y. Li, J. Huang and H. Tang, "A compliant parallel XY micromotion stage with complete kinematic decoupling." *IEEE Trans. Auto. Sci. & Eng*, vol. 9, no.3, pp. 538-553, Jul. 2012.

[16] Y. Du, T. Li, Y. Jiang, and H. Wang, "Design and analysis of a 2-degree-of-freedom flexure-based micro-motion stage," *Advances in Mechanical Engineering*, vol. 8, no.3, pp. 1-13, 2016.

[17] W. Zhu, Z. Zhu, Y. Shi, X. Wang, K. Guan and B. Ju, "Design, modeling, analysis and testing of a novel piezo-actuated XY compliant mechanism

for large workspace nano-positioning," *Smart Mater Struct*, vol. 25, no.11, pp. 115033, 2016.

[18] Y. Qin, B. Shirinzadeh, Y. Tian and D. Zhang, "Design issues in a decoupled XY, stage: Static and dynamics modeling, hysteresis compensation, and tracking control," *Sensor Actuat A-Phys*, vol. 194, no.5, pp. 95-105, 2013.

[19] S. Wan and Q. Xu, "Design and analysis of a new compliant XY micropositioning stage based on Roberts mechanism," *Mech. Mach. Theory*, vol. 95, pp. 125-139, Jan. 2016.

[20] G. Gu, L. Zhu, C. Su, H. Ding and S. Fatikow, "Modeling and control of piezo-actuated nanopositioning stages: a survey," *IEEE Trans. Autom. Sci. Eng*, vol. 13, no. 1, pp. 313-332, Jan. 2014.

[21] Y. Qin, B. Shirinzadeh, Y. Tian, D. Zhang and U. Bhagat, "Design and Computational Optimization of a Decoupled 2-DOF Monolithic Mechanism," *IEEE/ASME Trans. Mechatronics*, vol. 3, no. 19, pp. 872-881, Jun. 2014.

[22] Y. Li, S. Xiao, L. Xi and Z. Wu, "Design, modeling, control and experiment for a 2-DOF compliant micro-motion stage," *Inter J Prec. Eng. Man*, vol. 15, no. 4, pp. 735-744, Apr. 2014.

[23] Y. Qin, B. Shirinzadeh, D. Zhang and Y. Tian, "Design and kinematics modeling of a novel 3-dof monolithic manipulator featuring improved scott-russell mechanisms," *Journal of Mechanical Design*, vol. 135, no.10, pp. 1-9, June 2013.

[24] H. Tang, J. Gao, X. Chen, K. Yu, S. To, Y. He, X. Chen, Z. Zeng, S. He, C. Chen and Y. Li, "Development and Repetitive-compensated PID Control of a Nanopositioning Stage with Large-Stroke and Decoupling Property," *IEEE Trans. Ind. Electron.*, vol. 65, no. 5, pp. 3995–4005, May. 2018.

[25] Q. Xu and Y. Li, "Analytical modeling, optimization and testing of a compound bridge-type compliant displacement amplifier," *Mech. Mach. Theory*, vol. 46, no. 2, pp. 183-200, Feb. 2011.

[26] Y. Li and Q. Xu, "Design and Analysis of a Totally Decoupled Flexure-Based XY Parallel Micromanipulator", *IEEE Trans. Robot*, vol. 25, no.3, pp. 645-657, June 2009.

[27] W. Zhu, Z. Zhu, P. Guo and B. Ju, "A novel hybrid actuation mechanism based XY nanopositioning stage with totally decoupled kinematics." *Mech. Syst. Signal Process.*, vol. 99, pp. 747-759, May.2018.

[28] P. Liu and P. Yan, "A new model analysis approach for bridge-type amplifiers supporting nano-stage design," *Mech. Mach. Theory*, vol. 99, pp. 176-188, Jan. 2016.

[29] F. Wang, C. Liang, Y. Tian, X. Zhao and D. Zhang, "A flexure-based kinematically decoupled micropositioning stage with a centimeter range dedicated to micro/nano manufacturing," *IEEE/ASME Trans. Mechatronics*, vol. 21, no. 2, pp. 1055–1062, Apr. 2016.

[30] F. Wang, X. Zhao, D. Zhang, Y. Wu, B. Shirinzadeh and Y. Tian, "Design and control of a high-acceleration precision positioning system with a novel flexible decoupling mechanism", *PIMechE , Part C, Journal of Mechanical Engineering Science*, vol. 224, no.2, pp. 431-442, 2010.

[31] Y. Qin, B. Shirinzadeh, D. Zhang and Y. Tian, "Compliance modeling and analysis of statically indeterminate symmetric flexure structures". *Precision Engineering*, vol. 37, no.2, pp. 415-424, Apr. 2013.

[32] X. Sun, W. Chen, Y. Tian, S. Fatikow, R. Zhou, J. Zhang and M. Mikczinski, "A novel flexure-based microgripper with double amplification mechanisms for micro/nano manipulation," *Rev. Sci. Instrum.*, vol. 84, pp. 957-978, Aug. 2013.

[33] Y. K. Yong, B. Bhikkaji, S. O. R. Moheimani. "Analog control of a high-speed atomic force microscope scanner", in *IEEE/ASME International Conference on Advanced Intelligent Mechatronics*, vol.32, pp.646-651, Sep. 2011.

[34] G. Schitter, P. J. Thurner, and P. K. Hansma, "Design and input-shaping control of a novel scanner for high-speed atomic force microscopy". *Mechatronics*, vol. 18, no. 5, pp. 282-288, 2008.